




Manipulation of the Rashba spin-orbit coupling of a distorted 1T-phase Janus WSSe monolayer: Dominant role of charge transfer and orbital components

Wenzhe Zhou ¹, Jianyong Chen ², Bei Zhang,^{3,4} Haiming Duan,⁴ and Fangping Ouyang ^{1,3,4,*}

¹State Key Laboratory of Powder Metallurgy, and Powder Metallurgy Research Institute, Central South University, Changsha 410083, People's Republic of China

²College of Science, Guilin University of Aerospace Technology, Guilin 541004, People's Republic of China

³School of Physics and Electronics, and Human Key Laboratory for Super-Microstructure and Ultrafast Process, Central South University, Changsha 410083, People's Republic of China

⁴School of Physics and Technology, Xinjiang University, Urumqi 830046, People's Republic of China



(Received 9 February 2021; revised 19 March 2021; accepted 22 March 2021; published 7 May 2021)

Janus monolayer materials, as the thinnest materials that may possess strong Rashba spin-orbit coupling, are helpful for the miniaturization of the charge-spin conversion devices. Using first-principles calculations, we investigated the structural stability and Rashba spin-orbit coupling of distorted 1T-phase Janus monolayer WSSe. Although the W atoms rotating around the Se atom are dynamically unstable in the stress-free state, the imaginary frequency disappears by applying a small compressive strain. From the perspectives of macroscopic charge transfer and microscopic atomic orbital compositions, the mechanism of the Rashba spin-orbit coupling strength of the distorted 1T-phase Janus monolayer WSSe was analyzed. The coupling strength can be greatly manipulated when -5 to 5% biaxial strain is applied. The charge transfer caused by the larger lattice constant and the rotation of the W atoms reduce the gradient of the potential so that the greater the electric polarization, the weaker the spin-orbit coupling. The coupling strength of different electronic states is determined by the proportion of the out-of-plane atomic orbitals, where d_{xz} and d_{yz} orbitals play the dominant role. These results contribute to the design of materials with greater Rashba spin-orbit coupling and the understanding of its mechanism.

DOI: [10.1103/PhysRevB.103.195114](https://doi.org/10.1103/PhysRevB.103.195114)

I. INTRODUCTION

As one of the branches of spintronics, spin-orbit coupling plays an important role in the field of charge-spin conversion [1,2]. Various nontrivial physical phenomena caused by this relativistic effect in related materials have been observed, such as spin Hall effect [3,4], spin galvanic effect [5], spin field effect transistors [6], and spin quantum computing [7]. For one, the Rashba effect originates from inversion asymmetry of structure and generally brings extraordinary phenomena on the surface or interface of materials [8]. In addition, Rashba spin-orbit coupling is easier to control, and it can be easily realized in experiment to regulate the device performance based on this effect.

Due to the reversible spontaneous polarization and the inherent Rashba effect, ferroelectric Rashba semiconductors have stimulated the interest of researchers [9–11]. However, low-dimensional ferroelectric materials are still scarce [12,13], which greatly limits the application in the miniaturization of Rashba devices. Recently, more and more single-layer ferroelectric materials have been predicted, and their spin-orbit coupling effects have also been studied [14,15]. As a representative of two-dimensional materials, transition metal dichalcogenides have been verified for their ferroelec-

tric properties in different phases [16–18]. The 1T-phase transition metal dichalcogenides are dynamically unstable but can be stabilized by the distortion of metal ions into trimers or zigzag chains. Different from the 2H-phase with mirror symmetry, the trimeric distortion of 1T-phase transition metal dichalcogenides destroy the inversion symmetry, producing spontaneous polarization and intrinsic Rashba spin-orbit coupling, which can be used as ferroelectric Rashba semiconductors [19,20]. In general, the strength of the spin-orbit coupling is proportional to the spontaneous polarization caused by symmetry breaking. For the trimeric distorted structures, the Rashba spin-orbit coupling is determined by the degree of distortion.

Although the electric polarization is nonreversible, Janus monolayer materials have been successfully prepared experimentally and theoretically predicted to have tunable large Rashba parameters, such as BiTeCl and BiTeBr layers [21], transition-metal dichalcogenides [22–24], group IV transition metal trichalcogenides [25], binary hexagonal nanosheets [26,27], and so on [28]. Janus monolayer materials are expected to be the thinnest materials with larger Rashba spin-orbit coupling. Among them, Janus transition metal chalcogenides have received the most attention due to the unique electronic properties [29,30], such as spin-valley locking, excitation phenomena, and phase transitions between various structures. The Janus structures of various phases of transition metal dichalcogenides have also been considered

*Corresponding author: ouyangfp06@tsinghua.org.cn

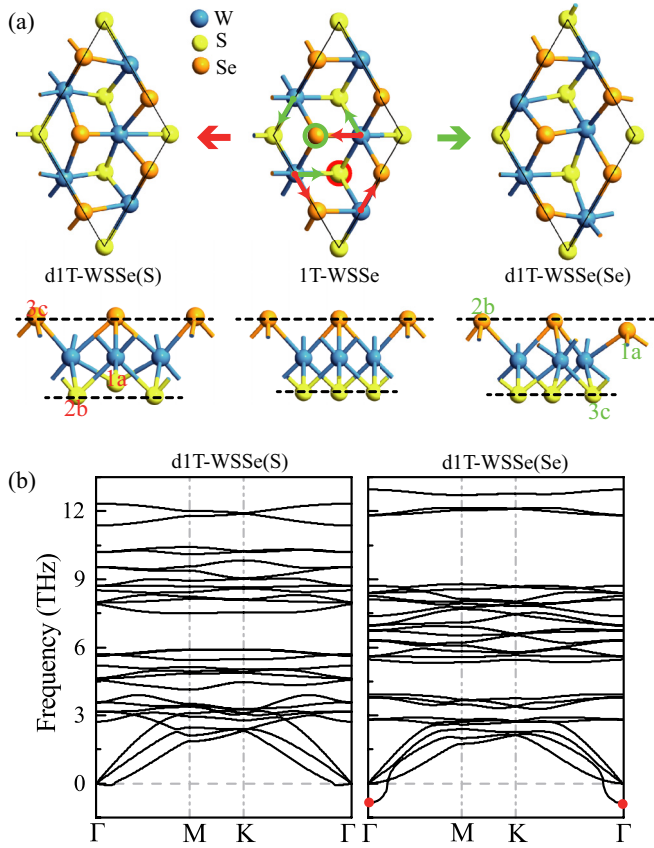


FIG. 1. (a) The W atoms rotate around the S atom (red arrows) or around the Se atom (green arrows), transforming the Janus monolayer WSSe from 1T to d1T phase, which are expressed as d1T-WSSe(S) and d1T-WSSe(Se), respectively. (b) The phonon spectrums of d1T-WSSe(S) and d1T-WSSe(Se).

[31,32]. Transition metal dichalcogenides exhibit Rashba spin splitting based on their Janus structure, and trimeric distortion further changes the spin-orbit field.

Rashba spin-orbit coupling is tunable under different external circumstances. The electrical control of gate voltage is the most widely used, which has been studied in many experiments and played an important role in spin field effect transistors [33–35]. Ignoring the effect of charge screening, the spin-orbit field includes the external electric field, and the coupling strength can be proportionally manipulated. The

TABLE I. The lattice parameters (a), bond lengths between W and S atoms (d_{W-S}), bond lengths between W and Se atoms (d_{W-Se}), the vertical distances between W and S atoms (h_{W-S}), and vertical distances between W and Se atoms (h_{W-Se}) of Janus monolayer 1T-WSSe, d1T-WSSe(S), and d1T-WSSe(Se).

	a (Å)	d_{W-S} (Å)	d_{W-Se} (Å)	h_{W-S} (Å)	h_{W-Se} (Å)
1T-WSSe	5.58	2.42	2.57	1.55	1.78
d1T-WSSe(S)	5.72	2.41(2b)	2.67	1.63(2b)	1.72
		3.67(1a)	2.42	1.09(1a)	
d1T-WSSe(Se)	5.74	2.31	2.53(2b)	1.53	1.79(2b)
		4.05	2.60(1a)		1.35(1a)

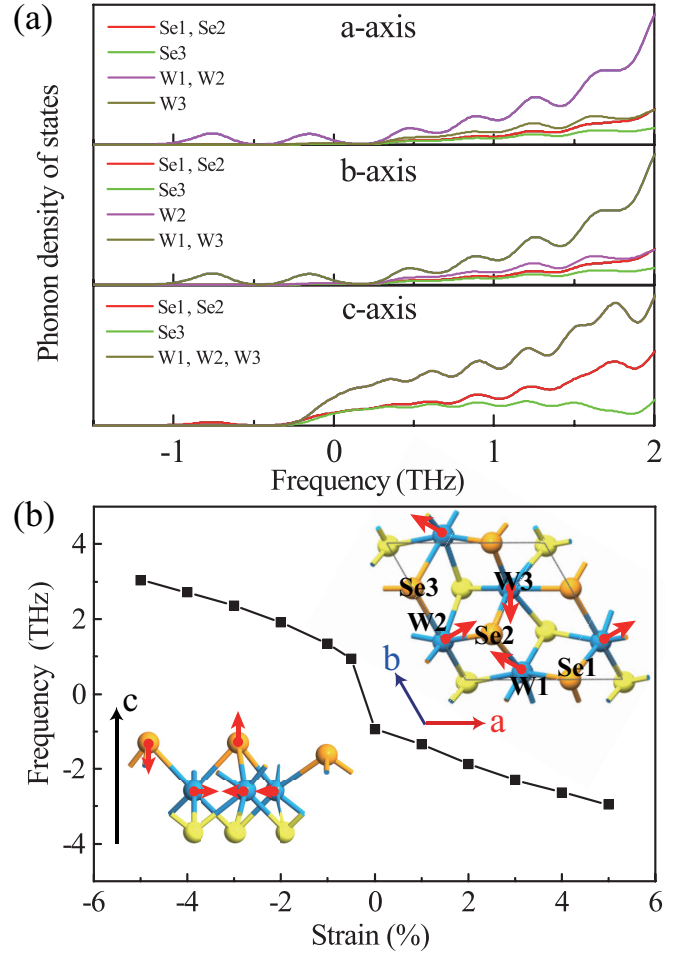


FIG. 2. (a) The projected phonon density of states of monolayer d1T-WSSe(Se). The direction of projection and the labels of atoms are shown in the insets of (b). (b) The frequency of the intrinsic unstable vibration mode at the Γ point changes with the strain, and the negative value indicates the instability. The insets are the atomic vibration images of the unstable phonon mode.

magnetic field also affects the intrinsic spin-orbit coupling and changes the properties of spin splitting and spin transport [36–38]. Strain [39] and doping [40] can affect orbital interactions or charge distribution and regulate the spin-orbit field. Proximity effects [41] and interlayer interactions [42,43] are also resources to produce or regulate Rashba spin-orbit coupling, which stems from asymmetric electrostatic interaction or charge transfer. Charge transfer can be regarded as a macro way to regulate electric polarization and built-in electric field, and it is often used to qualitatively analyze the change of Rashba coupling. However, the analysis of the Rashba effect of different electronic states of a certain material is still lacking. It has been proposed that orbital angular momentum is the causation of the Rashba effect [27,44]. Orbital angular momentum not only determines the splitting energy of spin-orbit coupling, but also has important significance for Rashba parameters. Therefore, it can be inferred that the different Rashba parameters of each electronic state are derived from the atomic orbital composition.

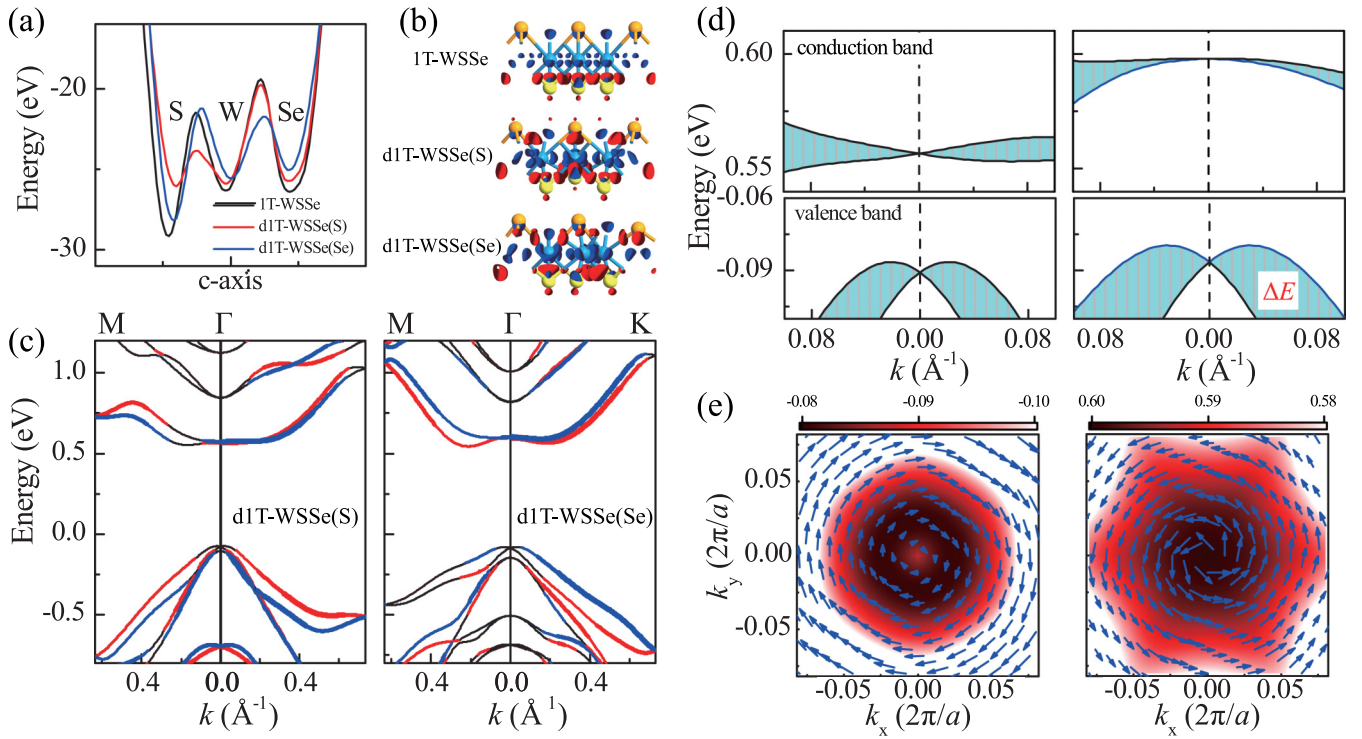


FIG. 3. (a) The average electronic potential energy in the vertical direction of monolayer 1T-WSSe, d1T-WSSe(S), and d1T-WSSe(Se). (b) The differential charge density of monolayer 1T-WSSe (up), d1T-WSSe(S) (middle), and d1T-WSSe(Se) (down). The red and blue represent the accumulation and depletion of electrons, respectively. (c) The band structures of monolayer d1T-WSSe(S) (left) and d1T-WSSe(Se) (right) with spin-orbit coupling. The red and blue weighted solid circles represent the spin direction along the positive and negative y directions, respectively. (d) The magnified views of the bottom conduction bands and the top valence bands of monolayer d1T-WSSe(S) (left) and d1T-WSSe(Se) (right), showing the spin splitting (splitting energy is ΔE) caused by spin-orbit coupling. (e) In-plane spin textures near the Γ point for the top valence band (left) and the bottom conduction band (right) of monolayer d1T-WSSe(Se). The color scales refer to the band energy (eV) with respect to the Fermi level.

Here, we investigated the manipulation of the Rashba spin-orbit coupling of distorted 1T-phase Janus monolayer WSSe and demonstrated two contributions, which are macroscopic charge transfer and microscopic orbital components. Based on first-principles study, the structural stability and electronic structure of distorted 1T-phase Janus monolayer WSSe were calculated. The distortion makes the electron transfer to the side of the distorting center, but the larger the electric polarization, the smaller the spin-orbit field. The tensile strain increases the Rashba parameter at the Γ point of the top valence band. For the systems with out-of-plane polarization, Rashba spin-orbit coupling produces in-plane spin splitting, while out-of-plane orbits have greater contributions to the coupling parameters. Here, d_{xz} and d_{yz} orbitals play a leading role in a distorted 1T-phase Janus WSSe monolayer when the strain is large enough.

II. COMPUTATIONAL DETAILS

The structural optimization and the iterative calculations in this paper were all performed through the Vienna *ab initio* Simulation Package (VASP) based on density functional theory (DFT) [45], which is the most widely used method to study the microscopic electronic structures of various materials. The phonon spectrum and vibration characteristics were calculated and analyzed using the density functional perturbation

theory method combined with the Phonopy tools [46]. A $3 \times 3 \times 1$ superlattice was used to calculate the dynamical matrix, and a $15 \times 15 \times 1$ q-mesh was adopted to obtain the phonon density of states. The projector augmented wave scheme and plane-wave basis set with an energy cutoff of 600 eV were employed [47]. The exchange-correlation effect was treated by the generalized gradient approximation of the Perdew-Burke-Ernzerhof functional [48]. A vacuum region of 30 Å was applied along the z direction so that the interaction between repeated slabs could be ignored and the influence of electrical polarization in the periodic structure was minimized. Nevertheless, to ensure accuracy, the dipole correction was applied to correct the errors introduced by the periodic boundary conditions [49]. The structural optimization was finished until the force on each atom was <0.001 eV/Å. The electronic self-consistent iteration stops until the energy difference between the two adjacent steps was $<10^{-6}$ eV, and a $11 \times 11 \times 1$ Γ -centered k-point grid was adopted.

III. RESULTS AND DISCUSSION

The distorted 1T-phase monolayer transition metal dichalcogenides were obtained from the corresponding unstable 1T-phase monolayers by rotating the transition metal atoms around the chalcogenide atoms, as shown in Fig. 1(a). Due to the different rotation centers of metal atoms, there

are two different structures of distorted 1T-phase Janus monolayer WSSe, which are labeled as d1T-WSSe(S) and d1T-WSSe(Se), respectively. For 1T-phase Janus monolayer WSSe transformed to d1T-WSSe(S), three W atoms in the $\sqrt{3} \times \sqrt{3} \times 1$ unit cell rotate anticlockwise around one S atom and clockwise around the other S atom (labeled as 2b), which get away from the third S atom (labeled as 1a), and the three Se atoms are equivalent. It is similar for the transition from 1T-phase Janus monolayer WSSe to d1T-WSSe(Se), but at the center of the rotation are Se atoms. The structural parameters are listed in Table I. The rotation of W atoms expands the unit cell and greatly changes the relative position of the 1a chalcogenide atom to W atoms. The bond lengths between W and 1a chalcogenide atoms become larger, and the vertical distances are smaller. Previous studies have indicated that the most important effect of the distortion is the electron transfer to 1a chalcogenide atoms [19,50]. There are two bond lengths between W and 3c chalcogenide atoms: one becomes longer, and the other becomes shorter. The W-S bonds have already been lengthened from the equilibrium distance due to the asymmetric Janus structure. For monolayer d1T-WSSe(Se), one W-S bond length is so large that it may be unstable.

The vibration of d1T-phase Janus monolayer WSSe was studied. As shown in Fig. 1, the phonon spectrum of monolayer d1T-WSSe(S) has no imaginary frequency, which indicates that the structure is dynamically stable. However, monolayer d1T-WSSe(Se) is unstable with imaginary frequency near the Γ point, and it may become stable under certain conditions. The projected phonon density of states and the atomic vibration images of the phonon with imaginary frequency are illustrated in Fig. 2. For the unstable mode, the three W atoms rotate clockwise in the plane, and the two Se atoms (labeled as 2b) move in opposite directions in the vertical plane. The unstable vibration is an optical branch and corresponds to the lattice being larger or smaller. It is assumed that the in-plane strain may change this virtual frequency and make the vibration stable. The frequency as a function of the in-plane biaxial strain was calculated. It was confirmed that the virtual frequency disappears when a little compressive strain is applied.

The electronic structures in Fig. 3 indicate that there is large Rashba spin splitting at the high symmetry points in reciprocal space. The Rashba spin-orbit coupling results in the in-plane spin splitting and band energy splitting. At a simple glance, monolayer d1T-WSSe(Se) possesses a greater spin-orbit coupling strength than d1T-WSSe(S) at the Γ point of the top valence band. The spin vortex in reciprocal space is shown in Fig. 3(e), which is an important feature of Rashba spin splitting, and the spin directions of the top valence band and the bottom conduction band are opposite. For 1T-phase Janus WSSe, the electric polarization points from S layer to Se layer due to S atoms gaining electrons. The rotation of W atoms brings the electron transfer to the 1a chalcogenide atom, leading to the larger electric polarization of d1T-WSSe(S) than d1T-WSSe(Se). The Rashba spin-orbit coupling strength is positively related to the electric polarization. However, the spin-orbit coupling strength of the Janus WSSe monolayer is not directly dominated by the polarization. The electronegativity of the S atom is so large that the accumulation of

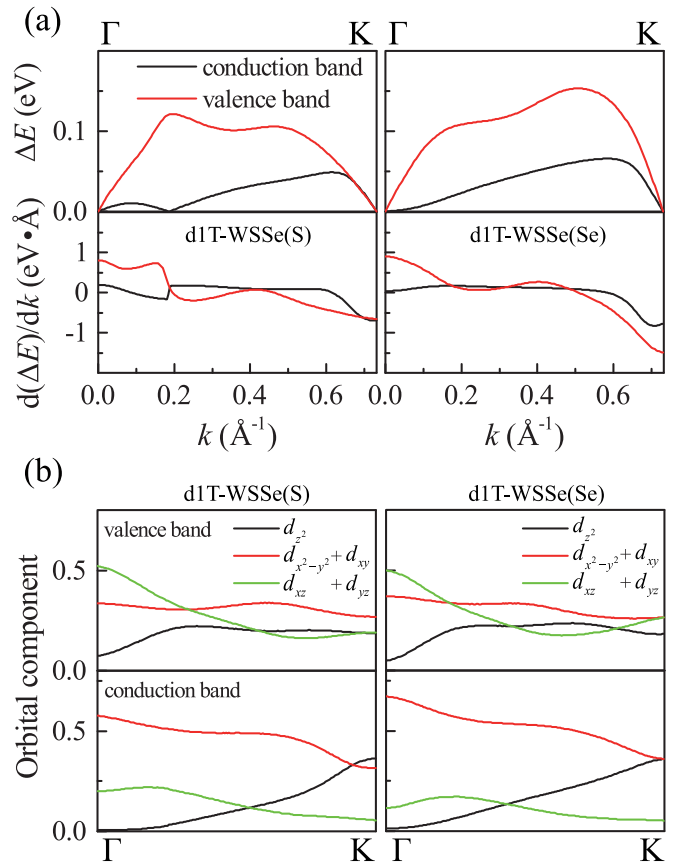


FIG. 4. (a) The energy splitting (ΔE) and the first derivative of the energy splitting to wave vector [$d(\Delta E)/dk$], (b) the compositions of atomic d orbitals of the top valence band and the bottom conduction band of d1T-WSSe(S) (left) and d1T-WSSe(Se) (right) monolayers.

electrons is not enough to offset the potential difference, which results in a low potential energy on the S side, and the built-in electric field (gradient of potential) is the same as the electric polarization, pointing from the S side to the Se side. As shown in Fig. 3(a), the electron transfer increases the potential energy of the S side in d1T-WSSe(S) and the Se side in d1T-WSSe(Se), which reduces and increases the gradient of the potential of d1T-WSSe(S) and d1T-WSSe(Se), respectively. Therefore, the asymmetry and gradient of potential is inversely proportional to the electric polarization. Meanwhile, the spin-orbit field is proportional to the gradient of potential. It is one of the macrolevel reasons for the larger Rashba spin-orbit coupling of monolayer d1T-WSSe(Se) than that of d1T-WSSe(S).

To quantitatively analyze the spin-orbit coupling strength, we calculate the splitting energy [ΔE in Fig. 3(d)] of the top valence band, the bottom conduction band, and the first derivative of the splitting energy to the wave vector, which are plotted in Fig. 4. According to the spin texture in a previous paper [20], only the Γ and K points have significant Rashba spin-orbit coupling, which does not exist at the M point. Therefore, the focus of the next discussion is on the spin-orbit coupling at the Γ and K points. The spin-orbit coupling strength near the high symmetry point of the reciprocal

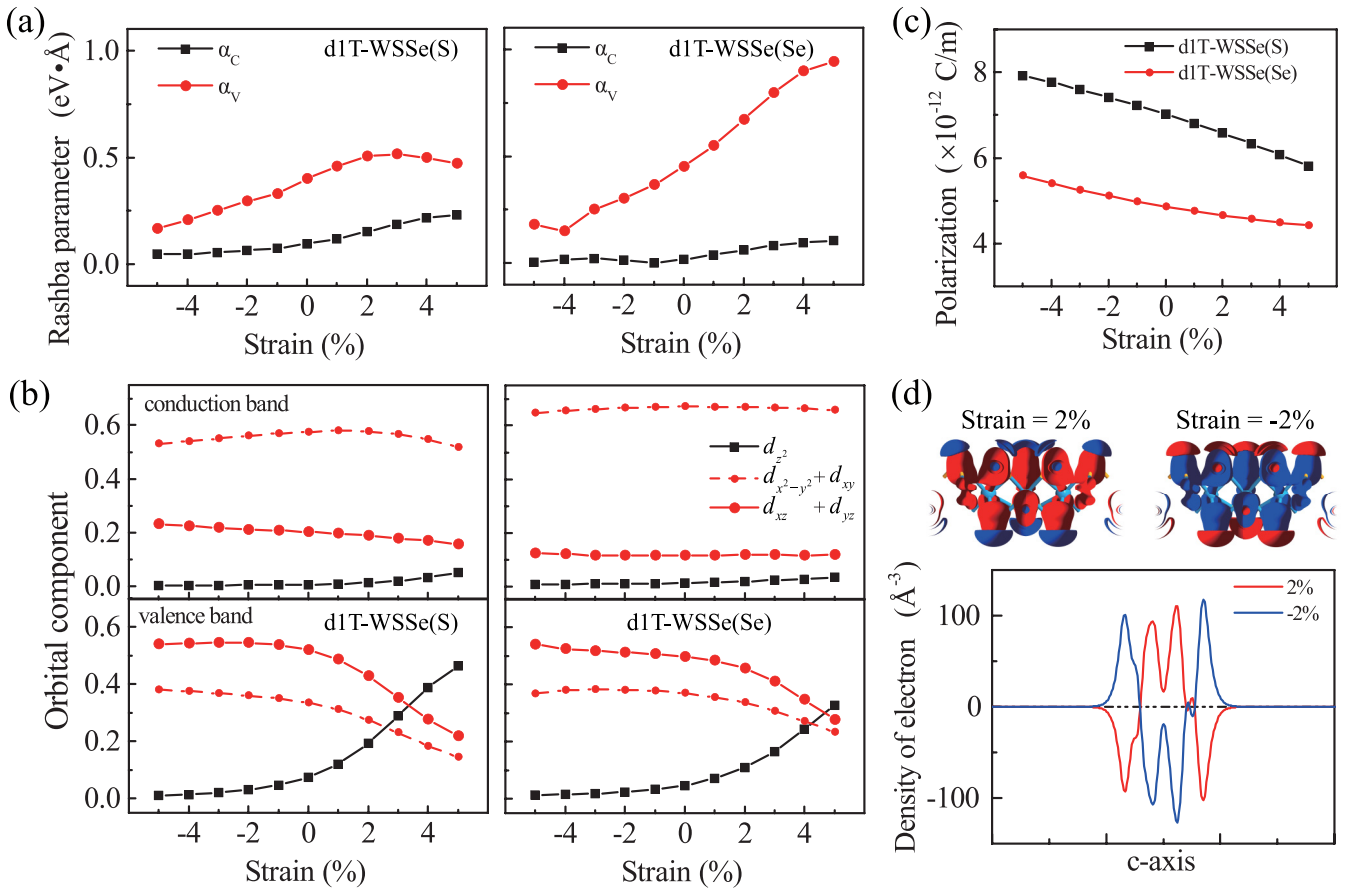


FIG. 5. (a) The strain regulated Rashba parameters at the Γ point of the top valence band and the bottom conduction band of monolayer d1T-WSSe(S) (left) and d1T-WSSe(Se) (right). (b) The changes of d orbital compositions at the Γ point of the top valence band and the bottom conduction band of monolayer d1T-WSSe(S) (left) and d1T-WSSe(Se) (right) as functions of the in-plane biaxial strain. (c) The polarizations of monolayer d1T-WSSe(S) and d1T-WSSe(Se) change with the in-plane biaxial strain. (d) The isosurface views (up) and the sum values along the c axis of differential electron density of the d1T-WSSe(S) monolayer when 2% compressive and tensile strain are applied. The red and blue in the isosurface views represent the accumulation and depletion of electrons, respectively.

space is valued as $\alpha_R = d[\Delta E(k)]/2dk$, which also contains nonlinear terms of spin-orbit coupling.

For the d1T-WSSe(S) monolayer, the top valence band possesses larger spin-orbit coupling strength than the bottom conduction band at the Γ point, and that is almost the same for the case of the K point. On the other hand, the spin-orbit coupling strengths of the top valence band at the Γ and K points are both larger than that of the bottom conduction band in the d1T-WSSe(Se) monolayer. Compared with the d1T-WSSe(S) monolayer, the coupling strengths of the top valence band of the d1T-WSSe(Se) monolayer are larger, while the strengths of the bottom conduction band are slightly smaller.

The crystal field determined by symmetry is an important origin of affecting the spin-orbit coupling [43]. The electronic states of different K points have different symmetries, which are reflected in the different orbital components. Considering the on-site spin-orbit coupling of atomic orbitals, the coupling strength of each K point is dominated by the corresponding composition of orbitals. When the electric polarization is along the z direction, the Rashba spin-orbit coupling induced spin splitting is in the xy plane, and the coupling strength is determined by the atomic orbital in the z direction because of the smaller orbital angular momentum in the z direction. At

the Γ point, the d_{z^2} orbit has no contribution to the bottom conduction band and a little contribution to the top valence band. The top valence band has larger spin-orbit coupling strength due to its larger component of d_{xz} and d_{yz} orbitals. The proportion of d_{xz} and d_{yz} orbitals at the K point decreases with the composition of d_{z^2} orbit increasing, which makes the coupling strength still sizable. Comparing d1T-WSSe(S) and d1T-WSSe(Se) monolayers, it is found that d_{xz} and d_{yz} orbitals are more important for Rashba spin-orbit coupling than the d_{z^2} orbit.

To confirm the relationship, the regulations of the spin-orbit coupling strength and the orbital composition at the Γ point of d1T-phase Janus monolayer WSSe were calculated. As shown in Fig. 5, overall, tensile strain enhances the strength of spin-orbit coupling, which is perfectly consistent with the change rule of orbital composition. The orbital compositions of the top valence band vary greatly with a tensile strain. The proportions of $d_{x^2-y^2}$, d_{xy} , and d_{xz} , d_{yz} orbitals decrease with the d_{z^2} orbit increasing, leading to the enhanced Rashba spin-orbit coupling. The coupling strength of d1T-WSSe(S) does not increase with increasing strain for the top valence band, due to the reduction of d_{xz} and d_{yz} orbitals. On the other hand, the compressive strain does not greatly affect

the orbital composition, but still significantly modulates the strength of spin-orbit coupling. From another perspective, the reason for the change of coupling strength is the macroscopic charge transfer. The S atom gets more electrons from the W atom, and the electric polarization becomes larger with a compressive strain. As discussed above, larger polarization corresponds to smaller gradient of potential and spin-orbit coupling strength.

IV. CONCLUSIONS

In summary, using first-principles research based on DFT, we investigated the dynamic stability and electronic structures of distorted 1T-phase Janus monolayer WSSe and focused on the regulation of Rashba spin-orbit coupling. In comparison, the W atoms prefer to rotate around S atoms, which makes the bond length between W and 1a S atoms longer, and the S atom gets more electrons. The charge transfer reduces the gradient of the potential, so it is concluded that the greater the macroscopic polarization, the weaker the Rashba spin-orbit coupling strength. On the other hand, the coupling strength at different electronic states in the reciprocal space is dominated by the orbital composition. For the case where the electric polarization is perpendicular to the two-dimensional material, the atomic

orbital in the z direction makes a greater contribution to the Rashba spin-orbit coupling, due to its larger orbital angular momentum in the x and y directions. As for the distorted 1T-phase Janus WSSe monolayers, d_{xz} and d_{yz} orbitals have greater importance than the d_{z^2} orbital to the strength of Rashba coupling. The regulation of Rashba spin-orbit coupling by strain is completely dominated by macroscopic charge transfer and microscopic orbital components.

ACKNOWLEDGMENTS

This paper was financially supported by the National Natural Science Foundation of China (Grant No. 52073308, No. 11804395), the Distinguished Young Scholar Foundation of Hunan Province (Grant No. 2015JJ1020), the Central South University Research Fund for Innovation-Driven Program (No. 2015CX51035) and the Central South University Research Fund for Sheng-hua scholars (Grant No. 502033019), Hunan Provincial Innovation Foundation for Postgraduates (Grant No. CX20190107), State Key Laboratory of Powder Metallurgy at Central South University, and the Fundamental Research Funds for the Central Universities of Central South University.

-
- [1] A. Avsar, H. Ochoa, F. Guinea, B. Özyilmaz, B. J. van Wees, and I. J. Vera-Marun, Colloquium: spintronics in graphene and other two-dimensional materials, *Rev. Mod. Phys.* **92**, 021003 (2020).
 - [2] J. C. R. Sánchez, L. Vila, G. Desfonds, S. Gambarelli, J. P. Attané, J. M. D. Teresa, C. Magén, and A. Fert, Spin-to-charge conversion using Rashba coupling at the interface between non-magnetic materials, *Nat. Commun.* **4**, 2944 (2013).
 - [3] J. Sinova, D. Culcer, Q. Niu, N. A. Sinitsyn, T. Jungwirth, and A. H. MacDonald, Universal Intrinsic Spin Hall Effect, *Phys. Rev. Lett.* **92**, 126603 (2004).
 - [4] J. Sinova, S. O. Valenzuela, J. Wunderlich, C. H. Back, and T. Jungwirth, Spin Hall effects, *Rev. Mod. Phys.* **87**, 1213 (2015).
 - [5] S. D. Ganichev, Spin-galvanic effect and spin orientation by current in non-magnetic semiconductors, *Int. J. Mod. Phys. B* **22**, 1 (2008).
 - [6] H. C. Koo, J. H. Kwon, J. Eom, J. Chang, S. H. Han, and M. Johnson, Control of spin precession in a spin-injected field effect transistor, *Science* **325**, 1515 (2009).
 - [7] C. Flindt, A. S. Sørensen, and K. Flensberg, Spin-Orbit Mediated Control of Spin Qubits, *Phys. Rev. Lett.* **97**, 240501 (2006).
 - [8] A. Manchon, H. C. Koo, J. Nitta, S. M. Frolov, and R. A. Duine, New perspectives for Rashba spin-orbit coupling, *Nat. Mater.* **14**, 871 (2015).
 - [9] S. Picozzi, Ferroelectric Rashba semiconductors as a novel class of, multifunctional materials, *Front. Phys.* **2**, 10 (2014).
 - [10] A. Narayan, Class of Rashba ferroelectrics in hexagonal semiconductors, *Phys. Rev. B* **92**, 220101(R) (2015).
 - [11] M. Liebmann *et al.*, Giant Rashba-type spin splitting in ferroelectric GeTe(111), *Adv. Mater.* **28**, 560 (2016).
 - [12] M. Dawber, K. M. Rabe, and J. F. Scott, Physics of thin-film ferroelectric oxides, *Rev. Mod. Phys.* **77**, 1083 (2005).
 - [13] Z. Guan, H. Hu, X. Shen, P. Xiang, N. Zhong, J. Chu, and C. Duan, Recent progress in two-dimensional ferroelectric materials, *Adv. Electron. Mater.* **6**, 1900818 (2020).
 - [14] D. D. Sante, A. Stroppa, P. Barone, M. H. Whangbo, and S. Picozzi, Emergence of ferroelectricity and spin-valley properties in two-dimensional honeycomb binary compounds, *Phys. Rev. B* **91**, 161401(R) (2015).
 - [15] J. Kim, K.-W. Kim, D. Shin, S.-H. Lee, J. Sinova, N. Park, and H. Jin, Prediction of ferroelectricity-driven berry curvature enabling charge- and spin-controllable photocurrent in tin telluride monolayers, *Nat. Commun.* **10**, 3965 (2019).
 - [16] Z. Fei, W. Zhao, T. A. Palomaki, B. Sun, M. K. Miller, Z. Zhao, J. Yan, X. Xu, and D. H. Cobden, Ferroelectric switching of a two-dimensional metal, *Nature* **560**, 336 (2018).
 - [17] P. Sharma, F. X. Xiang, D. F. Shao, D. Zhang, E. Y. Tsybal, A. R. Hamilton, and J. Seidel, A room-temperature ferroelectric semimetal, *Sci. Adv.* **5**, eaax5080 (2019).
 - [18] S. Yuan, X. Luo, H. L. Chan, C. Xiao, Y. Dai, M. Xie, and J. Hao, Room-temperature ferroelectricity in MoTe₂ down to the atomic monolayer limit, *Nat. Commun.* **10**, 1775 (2019).
 - [19] S. N. Shirodkar and U. V. Waghmare, Emergence of Ferroelectricity at a Metal-Semiconductor Transition in a 1T Monolayer of MoS₂, *Phys. Rev. Lett.* **112**, 157601 (2014).
 - [20] E. Bruyer, D. Di Sante, P. Barone, A. Stroppa, M.-H. Whangbo, and S. Picozzi, Possibility of combining ferroelectricity and Rashba-like spin splitting in monolayers of the 1T-type transition-metal dichalcogenides MX₂ ($M = \text{Mo, W}$; $X = \text{S, Se, Te}$), *Phys. Rev. B* **94**, 195402 (2016).
 - [21] D. Hajra, R. Sailus, M. Blei, K. Yumigeta, Y. Shen, and S. Tongay, Epitaxial synthesis of highly oriented 2D Janus Rashba

- semiconductor BiTeCl and BiTeBr layers, *ACS Nano* **14**, 15626 (2020).
- [22] A.-Y. Lu, H. Zhu, J. Xiao, C.-P. Chuu, Y. Han, M.-H. Chiu, C.-C. Cheng, C.-W. Yang, K.-H. Wei, Y. Yang, Y. Wang, D. Sokaras, D. Nordlund, P. Yang, D. A. Muller, M.-Y. Chou, X. Zhang, and L.-J. Li, Janus monolayers of transition metal dichalcogenides, *Nat. Nanotechnol.* **12**, 744 (2017).
- [23] J. Zhang, S. Jia, I. Kholmanov, L. Dong, D. Er, W. Chen, H. Guo, Z. Jin, V. B. Shenoy, L. Shi, and J. Lou, Janus monolayer transition-metal dichalcogenides, *ACS Nano* **11**, 8192 (2017).
- [24] R. Li, Y. Cheng, and W. Huang, Recent progress of Janus 2D transition metal chalcogenides: from theory to experiments, *Small* **14**, 1802091 (2018).
- [25] R. Ahammed, N. Jena, A. Rawat, M. K. Mohanta, Dimple, and A. D. Sarkar, Ultrahigh out-of-plane piezoelectricity meets giant Rashba effect in 2D Janus monolayers and bilayers of group IV transition-metal trichalcogenides, *J. Phys. Chem. C* **124**, 21250 (2020).
- [26] L. Zhu, T. Zhang, G. Chen, and H. Chen, Huge Rashba type spin orbit coupling in binary hexagonal Px nanosheets ($X = \text{As, Sb, and Bi}$), *Phys. Chem. Chem. Phys.* **20**, 30133 (2018).
- [27] M. Ünzelmann, H. Bentmann, P. Eck, T. Kißlinger, B. Geldiyev, J. Rieger, S. Moser, R. C. Vidal, K. Kißner, L. Hammer, M. A. Schneider, T. Fauster, G. Sangiovanni, D. D. Sante, and F. Reinert, Orbital-Driven Rashba Effect in a Binary Honeycomb Monolayer AgTe, *Phys. Rev. Lett.* **124**, 176401 (2020).
- [28] C. Zhang, Z. Sun, Y. Lin, L. Guan, and J. Tao, A 2D Rashba electron gas with large spin splitting in Janus structures of SnPbO₂, *Phys. Chem. Chem. Phys.* **22**, 11409 (2020).
- [29] K. Zhang, Y. Guo, Q. Ji, A.-Y. Lu, C. Su, H. Wang, A. A. Puzdov, D. B. Geohegan, X. Qian, S. Fang, E. Kaxiras, J. Kong, and S. Huang, Enhancement of van der Waals interlayer coupling through polar Janus MoSSe, *J. Am. Chem. Soc.* **142**, 17499 (2020).
- [30] H. Li, Y. Qin, B. Ko, D. B. Trivedi, D. Hajra, M. Y. Sayyad, L. Liu, S.-H. Shim, H. Zhuang, and S. Tongay, Anomalous behavior of 2D Janus excitonic layers under extreme pressures, *Adv. Mater.* **32**, 2002401 (2020).
- [31] M. Yagmurcukardes, C. Sevik, and F. M. Peeters, Electronic, vibrational, elastic, and piezoelectric properties of monolayer Janus MoSTe phases: a first-principles study, *Phys. Rev. B* **100**, 045415 (2019).
- [32] Y. Ma, L. Kou, B. Huang, Y. Dai, and T. Heine, Two-dimensional ferroelastic topological insulators in single-layer Janus transition metal dichalcogenides $MSSe$ ($M = \text{Mo, W}$), *Phys. Rev. B* **98**, 085420 (2018).
- [33] J. Hinz, H. Buhmann, M. Schäfer, V. Hock, C. R. Becker, and L. W. Molenkamp, Gate control of the giant Rashba effect in HgTe quantum wells, *Semicond. Sci. Technol.* **21**, 501 (2006).
- [34] K. Premasiri, S. K. Radha, S. Sucharitakul, U. R. Kumar, R. Sankar, F.-C. Chou, Y.-T. Chen, and X. P. A. Gao, Tuning Rashba spin-orbit coupling in gated multilayer InSe, *Nano Lett.* **18**, 4403 (2018).
- [35] L. Li, J. Zhang, G. Myeong, W. Shin, H. Lim, B. Kim, S. Kim, T. Jin, S. Cavill, B. S. Kim, C. Kim, J. Lischner, A. Ferreira, and S. Cho, Gate-tunable reversible Rashba-Edelstein effect in a few-layer graphene/2H-TaS₂ heterostructure at room temperature, *ACS Nano* **14**, 5251 (2020).
- [36] S. I. Erlingsson, J. C. Egues, and D. Loss, Energy spectra for quantum wires and two-dimensional electron gases in magnetic fields with Rashba and Dresselhaus spin-orbit interactions, *Phys. Rev. B* **82**, 155456 (2010).
- [37] C. H. L. Quay, T. L. Hughes, J. A. Sulpizio, L. N. Pfeiffer, K. W. Baldwin, K. W. West, D. Goldhaber-Gordon, and R. de Picciotto, Observation of a one-dimensional spin-orbit gap in a quantum wire, *Nat. Phys.* **6**, 336 (2010).
- [38] S. Q. Shen, M. Ma, X. C. Xie, and F. C. Zhang, Resonant Spin Hall Conductance in Two-Dimensional Electron Systems with a Rashba Interaction in a Perpendicular Magnetic Field, *Phys. Rev. Lett.* **92**, 256603 (2004).
- [39] T. Hu, F. Jia, G. Zhao, J. Wu, A. Stroppa, and W. Ren, Intrinsic and anisotropic Rashba spin splitting in Janus transition-metal dichalcogenide monolayers, *Phys. Rev. B* **97**, 235404 (2018).
- [40] J. Chen, K. Wu, H. Ma, W. Hu, and J. Yang, Tunable Rashba spin splitting in Janus transition metal dichalcogenide monolayers via charge doping, *RSC Adv.* **10**, 6388 (2020).
- [41] W. Zhou, Z. Yang, A. Li, M. Long, and F. Ouyang, Spin and valley splittings in Janus monolayer WSSe on a MnO(111) surface: large effective Zeeman field and opening of a helical gap, *Phys. Rev. B* **101**, 045113 (2020).
- [42] W. Zhou, J. Chen, Z. Yang, J. Liu, and F. Ouyang, Geometry and electronic structure of monolayer, bilayer, and multilayer Janus WSSe, *Phys. Rev. B* **99**, 075160 (2019).
- [43] T. P. Cysne, A. Ferreira, and T. G. Rappoport, Crystal-field effects in graphene with interface-induced spin-orbit coupling, *Phys. Rev. B* **98**, 045407 (2018).
- [44] S. R. Park, C. H. Kim, J. Yu, J. H. Han, and C. Kim, Orbital-Angular-Momentum Based Origin of Rashba-Type Surface Band Splitting, *Phys. Rev. Lett.* **107**, 156803 (2011).
- [45] G. Kresse and J. Furthmüller, Efficient iterative schemes for *ab initio* total-energy calculations using a plane-wave basis set, *Phys. Rev. B* **54**, 11169 (1996).
- [46] A. Togo and I. Tanaka, First principles phonon calculations in materials science, *Scr. Mater.* **108**, 1 (2015).
- [47] P. E. Blöchl, Projector augmented-wave method, *Phys. Rev. B* **50**, 17953 (1994).
- [48] J. P. Perdew, K. Burke, and M. Ernzerhof, Generalized Gradient Approximation Made Simple, *Phys. Rev. Lett.* **77**, 3865 (1996).
- [49] J. Neugebauer and M. Scheffler, Adsorbate-substrate and adsorbate-adsorbate interactions of Na and K adlayers on Al(111), *Phys. Rev. B* **46**, 16067 (1992).
- [50] J.-H. Choi and S.-H. Jhi, Origin of robust out-of-plane ferroelectricity in d1T-MoS₂ monolayer, *J. Phys. Condens. Matter* **32**, 045702 (2019).